Australasian Physical & Engineering Sciences in Medicine (2019) 42:665–670
https://doi.org/10.1007/s13246-019-00748-3

SCIENTIFIC PAPER

Ultrasound shear wave simulation of wave propagation at oblique angles

Dae Woo Park[1] · **Hyun-chong Cho**[2]

Received: 22 October 2018 / Accepted: 2 March 2019 / Published online: 15 March 2019

Abstract

Shear wave elasticity imaging (SWEI) has been used to measure the local tissue elasticity. The local tissue shear modulus can be reconstructed from the displacement field of shear waves using an algebraic Helmholtz inversion (AHI) equation or a time-of-flight (TOF)-based algorithm. The shear waves, which are generated by successive focusing of ultrasonic beams at different depths, propagate at oblique angles rather than along the lateral position. The wave propagation at oblique angles can result in bias in shear modulus reconstruction using the AHI equation or the TOF-based algorithm. In this study, the effect of wave propagation at oblique angles on the tissue shear modulus reconstruction was investigated using in silico finite element (FE) simulation. An FE elastic tissue with a hard inclusion model was designed. The shear waves with propagation angles of 0°, 5°, and 10° were applied to the model. The shear modulus and the percentage error in the model were computed using the AHI equation and the TOF-based algorithm at each propagation angle from 0° to 10°. For the AHI equation, the percentage error was 0% at propagation angles of 0° and 5°, and 1% at a propagation angle of 10° in the inclusion. In the surrounding tissue, the percentage error was 0% at propagation angles of 0°, 5°, and 10°. For the TOF-based algorithm, the percentage error was 0% at propagation angles of 0° and 5°, and 40% at a propagation angle of 10° in the inclusion. In the surrounding tissue, the percentage error was 0% at propagation angles of 0° and 5°, and 35% at a propagation angle of 10° in the inclusion. Therefore, whereas the TOF-based algorithm produced critical bias in shear modulus reconstruction by the shear wave propagation at oblique angles, the AHI equation was not affected by the propagation.

Keywords Shear modulus · Shear wave elasticity imaging · Time of flight · Ultrasound · Wave propagation

Introduction

Shear wave elasticity imaging (SWEI) has been utilized for noninvasive measurement of local tissue stiffness [1]. The tissue shear modulus is closely related to the propagation speed of shear waves [1, 2]. The mechanical vibration [3] or transient ultrasound (US) radiation force excitation [1, 2, 4] has been utilized to produce the shear waves. The tissue shear modulus can be reconstructed from the displacement field of shear waves using an algebraic Helmholtz inversion (AHI) equation [2, 4] or time-of-flight (TOF), including random sample consensus [5] and the Radon sum [6].

In SWEI, shear waves are created by successive focusing of ultrasonic beams at different depths [2]. For curvilinear arrays, shear waves travel at oblique angles when the push beam does not originate from the center of the transducer [7]. In this case, a multi-directional filter has been utilized to isolate shear waves propagation at oblique angles [8]. On the other hand, for linear arrays, the oblique angles of wave propagation are small and the bias of shear wave speed estimation has been usually ignored [7]. The AHI equation and the TOF-based algorithm estimate the shear modulus of tissues based on an assumption that shear waves travel along the lateral direction [2, 4–6]. Thus, the wave propagation at oblique angles can result in bias when estimating shear wave speed [5, 6, 9–11] and this could degrade accuracy of detecting malignant lesion in SWEI, especially in early stage of pathological changes [12, 13]. The quantification

✉ Hyun-chong Cho
hyuncho@kangwon.ac.kr

Dae Woo Park
bigrain@ncc.re.kr

[1] Division of Convergence Technology, National Cancer Center, Goyang-si, Republic of Korea

[2] Department of Electronic Engineering and Interdisciplinary Graduate Program for BIT Medical Convergence, Kangwon National University, Chuncheon-si, Republic of Korea

of error from the wave propagation at small oblique angles can improve accuracy of SWEI using the AHI equation or the TOF-based algorithm. So far, there is no report that comparing errors of shear modulus estimation between the AHI equation and TOF-based algorithm caused by the wave propagation at small oblique angles.

In this study, the effect of wave propagation at small oblique angles on the tissue shear modulus reconstruction was investigated using in silico finite element (FE) simulation. An FE elastic tissue with a hard inclusion model was designed. The shear waves with propagation angles of 0°, 5°, and 10° were applied to the model. The shear modulus of the inclusion and the surrounding tissue was computed at each propagation angle from 0° to 10° using the AHI equation and the TOF-based algorithm. The percentage errors of shear modulus in the inclusion and the surrounding tissue were calculated at each propagation angle.

Materials and methods

FE modeling

A 2D FE tissue model was designed using commercially available software (ANSYS Workbench 18.0, ANSYS Inc., Canonsburg, PA, USA). Figure 1 shows the schematic of the tissue model with dimensions and boundary conditions for FE simulations. A rectangular FE model with a length of 97 mm and a height of 60 mm was designed. A circular shape (10 mm diameter) inclusion was located 20 mm from the bottom surface and 38 mm from the right side of the model, as shown in Fig. 1. The 2D FE model was assumed to be isotropic and incompressible. The elastic moduli of inclusion and surrounding tissue were defined 10 kPa and 5 kPa, respectively, and Poisson's ratio was defined 0.495. The 2D FE tissue model was meshed using 2D triangular plane strain elements. The bottom boundaries of the tissue were fixed in all directions to prevent any bulk motion from the local body force excitation for shear wave generation. To create planar shear waves, consecutive body forces with time gap from 0 to 30 µs were applied downward over a 3 × 3 mm area through the entire tissue depth of the FE model for 180 µs. The wave propagation with angles of 0°, 5°, and 10° were generated by adjusting the time gap of consecutive body forces. Shear wave attenuation was not considered within the scope of the study. The *Y* displacements of shear waves over time were extracted over the entire *X* (across the body force direction) extent of the mesh. The temporal and spatial resolution of FE simulation were 125 µs and 0.2 × 0.2 mm, respectively.

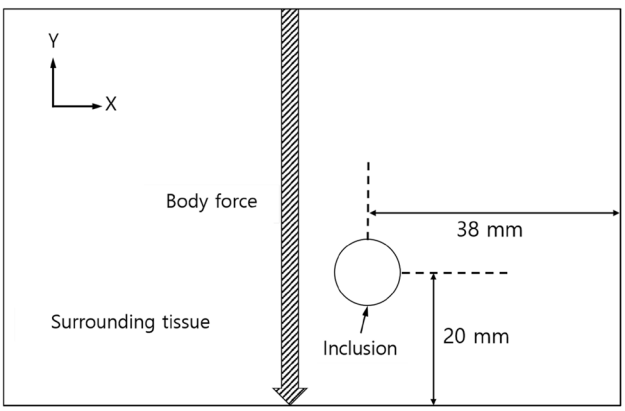

Fig. 1 Schematic of the tissue model with dimensions and boundary conditions for FE simulations

SWEI–modulus reconstruction

To remove wave reflections around the inclusion region, a 1D directional filter [8], which identifies the backward-moving shear waves in the *X* direction and eliminates the waves in the frequency domain, was applied to the *Y* displacement versus time data. The shear moduli of the inclusion and the surrounding tissue were reconstructed using the AHI equation and the TOF-based algorithm. In the TOF-based algorithm, the shear wave speed was determined from the *Y* displacement field by estimating the shear wave arrival time at each *X* position and calculating the slope of the position versus time data [6]. The slope was calculated using data from the positions within a 3-mm kernel in the *X* direction that was stepped across the *X* range. Shear wave speeds were reconstructed using a 3-mm kernel in the *Y* direction and then smoothed using a 2 mm × 2 mm median filter. The shear modulus (G) was calculated from the estimated shear wave speeds using the following equation:

$$G = \rho c^2 \tag{1}$$

where ρ is the density of medium and c is the speed of the shear wave. Each shear modulus for the hard inclusion and the surrounding tissue was spatially averaged within the area of the hard inclusion size. The average shear moduli of the inclusion and surrounding tissue were computed at each propagation angle up to 10°.

For the shear moduli in the inclusion and surrounding tissue, the Shapiro–Wilk test was performed to evaluate normality. An one-way ANOVA test was performed for the average shear moduli of the inclusion and surrounding tissue to compare the variation between each wave propagation angle.

Results

Figure 2 shows the axial displacement color maps of the 2D FE tissue model at propagation angles of 0°, 5°, and 10°, which were captured at 3.0 ms and 4.5 ms after the shear

waves were generated by body force. The red color represents the shear wave front, and the location of the inclusion is represented by a black dashed circle. The shear wave front advanced immediately after it was propagated into the inclusion area. Note that the dynamic range of the color map was adjusted to clearly display the shear wave front.

Figure 3a presents the reconstructed shear modulus maps of the FE tissue model calculated by the AHI equation at propagation angles of 0°, 5°, and 10°. Figure 3b presents the reconstructed shear modulus maps of the FE tissue model calculated using the TOF-based algorithm at propagation angles of 0°, 5°, and 10°. The black dashed circle represents the boundary of the inclusion and the surrounding tissue. The shear modulus was spatially averaged in the inclusion and the surrounding tissue.

Figure 4a shows the average shear moduli of the inclusion (diagonal stripe pattern bar) and the surrounding tissue (solid bar) versus propagation angles of 0°, 5°, and 10° computed using the AHI equation. Figure 4b shows the average shear moduli of the inclusion and the surrounding tissue versus propagation angles of 0°, 5°, and 10° computed using the TOF-based algorithm. The input shear moduli of the inclusion and the surrounding tissue were denoted as red and blue dashed lines, respectively.

The error bar represents the standard deviation of the spatially averaged shear modulus for the inclusion and the surrounding tissue. In the AHI equation, at 0° propagation angle, the average shear moduli of the inclusion and the surrounding tissue were 3.3 ± 0.2 kPa and 1.7 ± 0.1 kPa, respectively. At a 5° propagation angle, the average shear moduli of the inclusion and the surrounding tissue were 3.3 ± 0.2 kPa and 1.7 ± 0.1 kPa, respectively. At a 10° propagation angle, the average shear moduli of the inclusion and the surrounding tissue were 3.3 ± 0.2 kPa and 1.7 ± 0.1 kPa, respectively. Both the shear moduli of the inclusion and the surrounding tissue had normal distribution with $p > 0.05$. The average shear moduli of the inclusion and the surrounding tissue were not significantly different for 0°, 5°, and 10° propagation angles. In the TOF-based algorithm, at a 0° propagation angle, the average shear moduli of the inclusion and the surrounding tissue were 3.3 ± 0.3 kPa and 1.7 ± 0.1 kPa, respectively. At a 5° propagation angle, the average shear moduli of the inclusion and the surrounding tissue were 3.4 ± 0.4 kPa and 1.7 ± 0.1 kPa, respectively. At a 10° propagation angle, the average shear moduli of the inclusion and the surrounding tissue were 4.7 ± 0.3 kPa and 2.3 ± 0.1 kPa, respectively. Both the shear moduli of the inclusion and the surrounding tissue had normal distribution with $p > 0.05$. The average shear moduli of the inclusion and the surrounding tissue were not significantly different between 0° and 5° propagation angles. However, both the average shear moduli of the inclusion and the surrounding tissue significantly different between 5° and 10° propagation

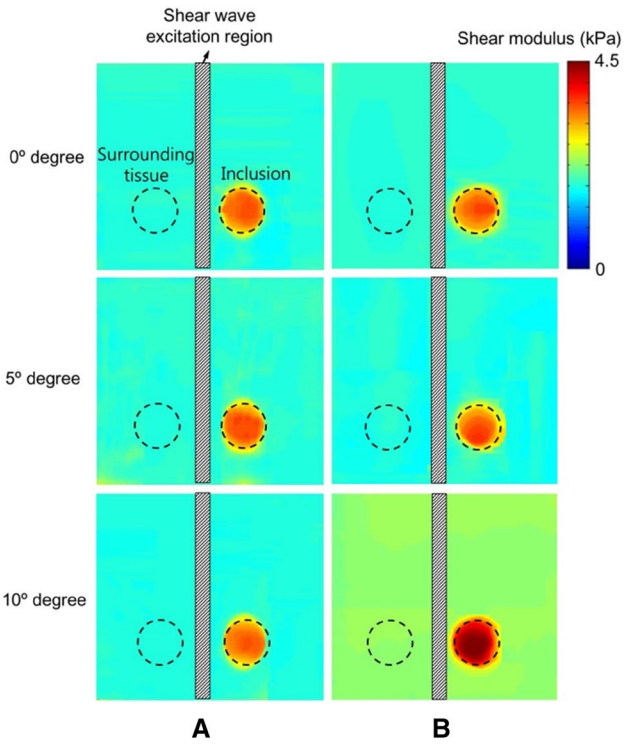

Fig. 3 Reconstructed shear modulus maps of the FE tissue model at propagation angles of 0°, 5°, and 10° using **a** the AHI equation and **b** the TOF-based algorithm

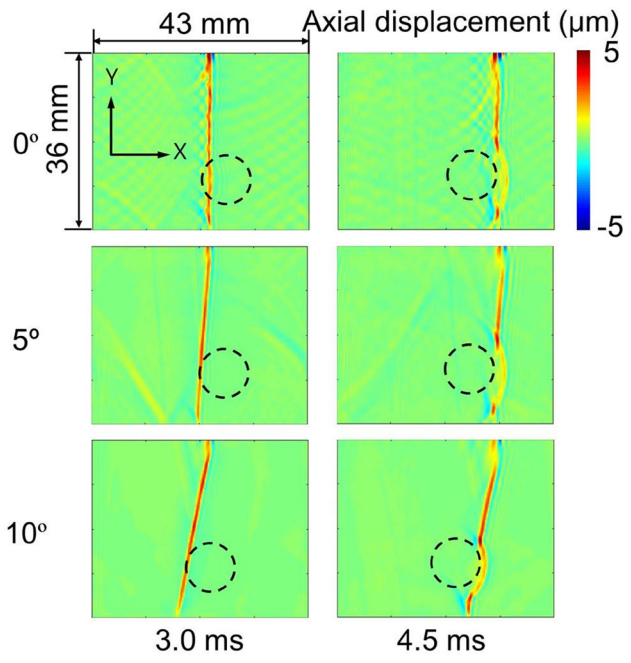

Fig. 2 Axial displacement color maps for propagation angles of 0°, 5°, and 10° at 3.0 ms and 4.5 ms after the shear waves were generated by body force

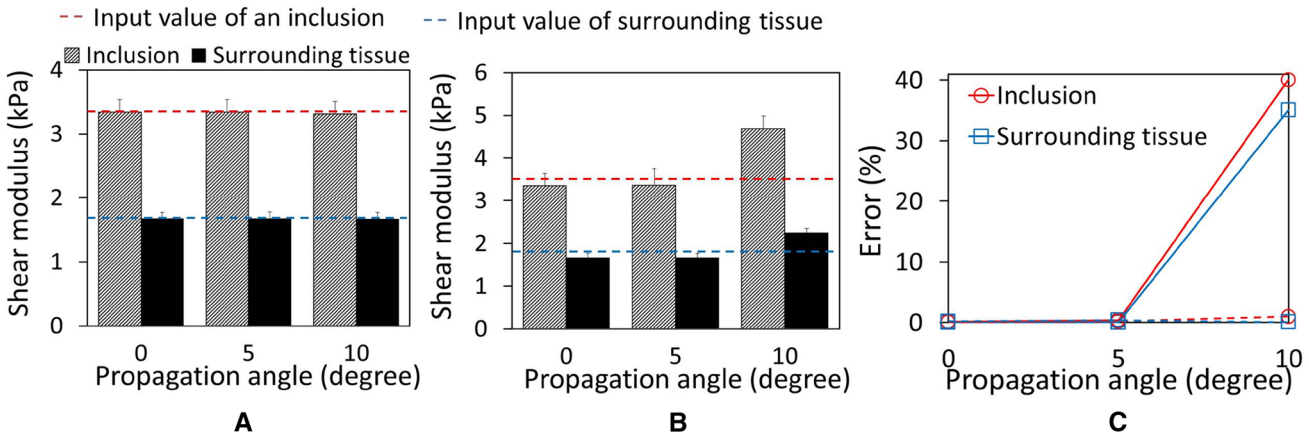

Fig. 4 Shear moduli of the inclusion and the surrounding tissue at propagation angles of 0°, 5°, and 10° computed using **a** the AHI equation and **b** the TOF-based algorithm. **c** Percentage errors of shear modulus in the inclusion and the surrounding tissue at propagation angles of 0°, 5°, and 10°

angles ($p < 0.05$). Figure 4c presents the percentage error of the shear modulus versus the propagation angles of 0°, 5°, and 10°.

The percentage errors of the inclusion and surrounding tissue are represented as open red circles and open blue squares, respectively. The solid and dashed lines represent the percentage errors for the TOF-based algorithm and AHI equation, respectively. For the AHI equation, the percentage error was 0% at propagation angles of 0° and 5°, and 1% at a propagation angle of 10° in the inclusion. In the surrounding tissue, the percentage error was 0% at propagation angles of 0°, 5°, and 10°. For the TOF-based algorithm, the percentage error was 0% at propagation angles of 0° and 5°, and 40% at a propagation angle of 10° in the inclusion. In the surrounding tissue, the percentage error was 0% at propagation angles of 0° and 5°, and 35% at a propagation angle of 10° in the inclusion.

Discussion

The errors of the tissue shear modulus computed by the TOF-based algorithm were much higher than those computed by the AHI equation for the oblique wave propagation. In the AHI equation, the percentage errors were less than 1% at propagation angles of 0°, 5°, and 10° for both the inclusion and the surrounding tissue. In contrast, in the TOF-based algorithm, the percentage errors were over 30% at the propagation angle of 10° for both the inclusion and the surrounding tissue. The TOF methods are based on the shear wave arrival time at each lateral position [11], and the shear wave speed estimation was critically affected by the wave propagation at oblique angles. On the other hand, the AHI equation uses the frequency domain of the axial displacement field, and the shear modulus reconstruction was less dependent on the wave propagation angles.

Shear wave propagation angles over 10° produced critical biases of the shear modulus reconstruction using the TOF-based algorithm. For linear arrays, the wave propagation angle is usually over 10° and thus, the bias of shear modulus computation should be considered when using the TOF-based algorithm. In the TOF-based algorithm, the multi-directional filter [8], designed corresponding to each direction of the shear wave propagation, should be utilized to reduce the bias of shear modulus computation.

The overestimation of shear modulus in the inclusion and the surrounding tissue was observed at propagation angles of 10° (Fig. 4b). The TOF-based algorithm determines the shear wave speed from the axial displacement field by estimating the shear wave arrival time at each lateral position [11]. The shear wave propagation at oblique angles distorted the axial displacement field, and this may have caused a delay in the shear wave arrival time at each lateral position. Further studies are required to determine the reason for the overestimation of the shear modulus computation.

In this study, the FE model was designed with the hard inclusion and the surrounding tissue. The hard inclusion produced a higher error of shear modulus computation than the surrounding tissue for wave propagation at an oblique angle of 10° (Fig. 4c). The percentage error of shear modulus in the hard inclusion sharply increased from 5° to 10° wave propagation angles, and reached 40%. In contrast, the percentage error of shear modulus in the soft surrounding tissue increased up to 35% at the wave propagation angle of 10°. In the inclusion region, the shear wave propagation angle can vary significantly due to wave deflection and reflection [8]. Thus, the effect of oblique angles of wave propagation was higher in the hard inclusion region than in the surrounding tissue area.

There are several limitations of our FE simulation approach. First, the FE tissue model assumed linear elastic materials. However, soft tissues normally have nonlinear elasticity [14]. In future studies, the effect of nonlinear tissue elasticity on the reconstruction of shear modulus for wave propagation at oblique angles needs to be evaluated. Second, the anisotropy of tissue properties was not considered in the FE simulation. The shear wave speed is distinctly different according to orientation of shear wave propagation in skeletal muscle tissues due to its anisotropic mechanical properties [15]. We will further study the effect of the anisotropy on the tissue shear modulus estimation for wave propagation at oblique angles. Third, the speckle noise was not considered, and the axial displacement field of the shear wave were obtained by FE simulation. US images normally contain speckle noise [16], which affects the axial displacement estimation. This effect of speckle noise on shear modulus computation may need further investigation.

To sum up, the wave propagation at small oblique angles produced critical biases of the shear modulus reconstruction when using the TOF-based algorithm. To improve accuracy of the TOF-based shear modulus reconstruction, the multi-directional filter should be used even for the wave propagation at small oblique angles.

Conclusion

The in silico FE simulation of SWEI demonstrated that shear wave propagation at oblique angles produced a critical bias of the shear modulus reconstruction using the TOF-based algorithm. In addition, the hard inclusion produced higher overestimation of shear modulus computation than the surrounding tissue, for wave propagation at an oblique angle of 10°. This overestimation can cause a critical error in elasticity measurements for tissues including hard inclusions, such as breast cancer tissue. Therefore, to reduce the bias of shear modulus computation, the multi-directional filter should be utilized in the TOF-based shear modulus reconstruction.

Funding This work was supported by the National Research Foundation of Korea (NRF) grant funded by the Korea government (MSIT) (No. 2017R1E1A1A03070297) and the Ministry of Education, Science and Technology (MEST) (No. 2018R1D1A1B07046796).

Compliance with ethical standards

Conflict of interest There are no conflicts of interest to declare.

Ethical approval This article does not contain any studies with human participants or animals performed by any of the authors.

Informed consent All study participants provided informed consent, and the study design was approved by the appropriate ethics review board. We have read and understood your journal's policies, and we believe that neither the manuscript nor the study violates any of these.

References

1. Sarvazyan AP, Rudenko OV, Swanson SD, Fowlkes JB, Emelianov SY (1998) Shear wave elasticity imaging: a new ultrasonic technology of medical diagnostics. Ultrasound Med Biol 24(9):1419–1435
2. Bercoff J, Tanter M, Fink M (2004) Supersonic shear imaging: a new technique for soft tissue elasticity mapping. IEEE Trans Ultrason Ferroelectr Freq Control 51(4):396–409
3. Sandrin L, Fourquet B, Hasquenoph J, Yon S, Fournier C, Mal F, Christidis C, Ziol M, Poulet B, Kazemi F, Beaugrand M, Palau R (2003) Transient elastography: a new noninvasive method for assessment of hepatic fibrosis. Ultrasound Med Biol 29(12):1705–1713
4. Nightingale K, McAleavey S, Trahey G (2003) Shear-wave generation using acoustic radiation force: in vivo and ex vivo results. Ultrasound Med Biol 29(12):1715–1723
5. Wang MH, Palmeri ML, Rotemberg VM, Rouze NC, Nightingale KR (2010) Improving the robustness of time-of-flight based shear wave speed reconstruction methods using RANSAC in human liver in vivo. Ultrasound Med Biol 36:802–813
6. Rouze NC, Wang MH, Palmeri ML, Nightingale KR (2010) Robust estimation of time-of-flight shear wave speed using a radon sum transformation. IEEE Trans Ultrason Ferroelectr Freq Control 57(12):2662–2670
7. Deng Y, Rouze NC, Palmeri ML, Nightingale KR (2017) Ultrasonic shear wave elasticity imaging sequencing and data processing using a verasonics research scanner. IEEE Trans Ultrason Ferroelectr Freq Control 64(1):164–176
8. Song P, Manduca A, Zhao H, Urban MW, Greenleaf JF, Chen S (2014) Fast shear compounding using robust two-dimensional shear wave speed calculation and multi-directional filtering. Ultrasound Med Biol 40(6):1343–1355
9. Palmeri ML, Wang MH, Dahl JJ, Frinkley KD, Nightingale KR (2008) Quantifying hepatic shear modulus in vivo using acoustic radiation force. Ultrasound Med Biol 34:546–558
10. Tanter M, Bercoff J, Athanasiou A, Deffieux T, Gennisson JL, Montaldo G, Muller M, Tardivon A, Fink M (2008) Quantitative assessment of breast lesion viscoelasticity: initial clinical results using supersonic shear imaging. Ultrasound Med Biol 34:1373–1386
11. Manduca A, Lake DS, Kruse SA, Ehman RL (2003) Spatiotemporal directional filtering for improved inversion of MR elastography images. Med Image Anal 7(4):465–473
12. Park DW (2016) Ultrasound shear wave simulation of breast tumor using nonlinear tissue elasticity. Comput Math Methods Med 2016:1–6
13. Poynard T, Munteanu M, Luckina E, Perazzo H, Ngo Y, Royer L, Fedchuk L, Sattonnet F, Pais R, Lebray P, Rudler M, Thabut D, Ratziu V (2013) Liver fibrosis evaluation using real-time shear wave elastography: applicability and diagnostic performance using methods without a gold standard. J Hepatol 58(5):928–935
14. Erkamp RQ, Skovoroda AR, Emelianov SY, O'Donnell M (2004) Measuring the nonlinear elastic properties of tissue-like phantoms. IEEE Trans Ultrason Ferroelectr Freq Control 51(4):410–419

15. Gennisson JL, Deffieux T, Macé E, Montaldo G, Fink M, Tanter M (2010) Viscoelastic and anisotropic mechanical properties of in vivo muscle tissue assessed by supersonic shear imaging. Ultrasound Med Biol 36(5):789–801
16. Gupta S, Chauhan RC, Sexana SC (2004) Wavelet-based statistical approach for speckle reduction in medical ultrasound images. Med Biol Eng Comput 42(2):189–192